



Nanoscale

Graphene-Based Encapsulation of Liquid Metal Particles

Journal:	<i>Nanoscale</i>
Manuscript ID	NR-ART-07-2020-005263.R1
Article Type:	Paper
Date Submitted by the Author:	10-Sep-2020
Complete List of Authors:	Creighton, Megan; US Air Force Research Laboratory; National Academies of Sciences Engineering and Medicine, National Research Council Fellow Yuen, Michelle; US Air Force Research Laboratory; National Academies of Sciences Engineering and Medicine, National Research Council Fellow Morris, Nicholas; UES Inc; US Air Force Research Laboratory Tabor, Christopher; US Air Force Research Laboratory,

SCHOLARONE™
Manuscripts

Journal Name

ARTICLE TYPE

Cite this: DOI: 00.0000/xxxxxxxxxx

Graphene-Based Encapsulation of Liquid Metal Particles[†]

Megan A. Creighton,^{a,b} Michelle C. Yuen,^{a,b} Nicholas J. Morris,^{a,c} and Christopher E. Tabor^a

Received Date

Accepted Date

DOI: 00.0000/xxxxxxxxxx

Liquid metals are a promising functional material due to their unique combination of fluidity at room temperature and metallic properties. They are of interest in wide-ranging fields including stretchable and flexible electronics, reconfigurable devices, microfluidics, biomedicine, material synthesis, and catalysis. Transformation of bulk liquid metal into particles has enabled further advances by allowing access to a broader palette of fabrication techniques for device manufacture or by increasing area available for surface-based applications. For gallium-based liquid metal alloys, particle stabilization is typically achieved by the oxide that forms spontaneously on the surface, even when only trace amounts of oxygen are present. The utility of the particles formed is governed by the chemical, electrical, and mechanical properties of this oxide. To overcome some of the intrinsic limitations of the native oxide, it is demonstrated here for the first time that 2D graphene-based materials can encapsulate liquid metal particles during fabrication and imbue them with previously unattainable properties. This outer encapsulation layer is used to physically stabilize particles in a broad range of pH environments, modify the particles' mechanical behavior, and control the electrical behavior of resulting films. This demonstration of graphene-based encapsulation of liquid metal particles represents a first foray into the creation of a suite of hybridized 2D material coated liquid metal particles.

1 Introduction

Gallium can be alloyed with other low-melting-point metals to form a eutectic composition, resulting in a metal that is liquid at room temperature. Two of the most prevalent examples are 75.5% gallium and 24.5% indium (commonly known as EGaln), and 68.5% gallium, 21.5% indium, and 10% tin. The conductivity of such alloys ($3.4 \times 10^6 \text{ S}\cdot\text{m}^{-1}$ for EGaln) coupled with the intrinsic deformability of the liquid state is of significant interest for self-healing^{1–3} or reconfigurable circuitry,^{4–6} and stretchable, flexible or bio-integrated electronics.^{7–12}

Manufacturing such devices with bulk liquid metal can be challenging. The gallium within the alloys is known to react nearly instantaneously upon contact with oxygen and form a passivating skin layer that is electrically insulating and adherent to many surfaces.^{13,14} This reactivity with oxygen can instead be exploited to form discrete particles composed of an oxide encapsulating a liquid metal core. Much of the previous work on these applications utilize liquid metals in bulk form to ensure low electrical

resistances within the device.

However, the the increased contact resistance between the oxide surfaces of discrete particles suspended in a solvent (*i.e.* using an ink in lieu of bulk liquid metal) is often a favorable trade-off for increased compatibility with existing manufacturing processes.^{15,16} The surfaces of liquid metal particles can be modified by binding ligands or changing the surface oxide composition and thickness. This functionalization of the particle surface has been leveraged to increase ink stability,^{16–18} broaden substrate compatibility,¹⁹ and modify the response to mechanical input.^{20–22} Moreover, formation of liquid metal particles augments opportunities in surface-dependent applications such as drug delivery,^{23,24} biomedicine (e.g. photothermal treatment, antimicrobials),^{24–27} catalysis,^{28–30} metal oxide synthesis,^{29,31} and stimuli-responsive systems.³² Such applications are realized by functionalization of the liquid metal particle surface via electroplating,^{23,28} polymer encapsulation,²⁷ or powder coatings.^{24,33,34,34,35} For further discussion of liquid metals and their applications, the reader is directed to recent review articles.^{36–39}

While liquid metal particles show great promise for applications in many fields, even something as simple as exposure to water has been shown to change the composition⁴⁰ and weaken (*i.e.* decrease the surface yield stress)⁴¹ the oxide shell, which can have drastic implications for particle stability and thus utility. Strongly acidic or basic solvents are known to etch away the oxide shell and cause particle coalescence.⁴² It is therefore desirable to

^a Air Force Research Laboratory, Materials and Manufacturing Directorate, Wright-Patterson Air Force Base, Dayton, OH, USA. E-mail: {megan.creighton.ct; michelle.yuen.ct; nicholas.morris.19, christopher.tabor.1}@us.af.mil

^b National Research Council, Washington, District of Columbia 20001, USA.

^c UES Inc., Dayton, OH, USA.

[†] Electronic Supplementary Information (ESI) available. See DOI: 00.0000/00000000.

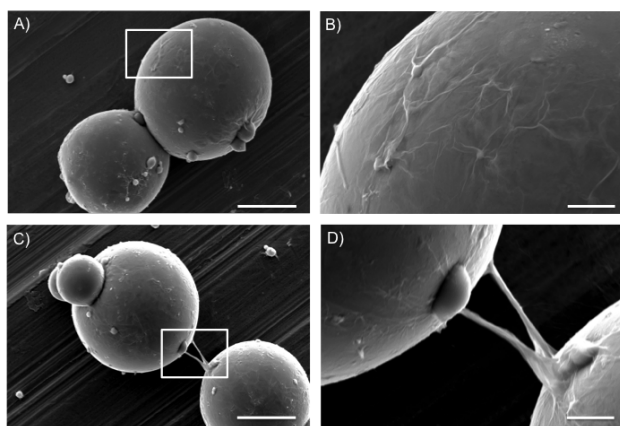


Fig. 1 A) Liquid metal particles formed in the presence of GO (scalebar = 5 μm). B) A close-up view of the surface shows a wrinkled morphology, characteristic of a GO encapsulation on a liquid surface (scalebar = 1 μm). C) A single sheet of GO can have different regions that interact with separate GaLMA particles, and can create a tether between them (scalebar = 5 μm). D) A close-up view of the tether, showing the twisting that occurred during processing (scalebar = 1 μm).

develop liquid metal particle formulations that are more robust to a broader range of conditions.

Inorganic coatings are anticipated to offer such utility, though their use in the encapsulation of liquid metals is less explored than molecular options. The first report of assembly of inorganic materials on the surface of liquid metal is believed to be first reported by Sivan, *et al.* for the formation of liquid metal marbles.³⁵ These powder-coated liquid metal droplets were often millimeter-sized and required a manual fabrication process to roll the liquid metal drops in a powder bed. This concept has been extended by Chen, *et al.*³⁴ for the macro-scale assembly of graphene powder coatings liquid metal droplets. More recently, Zhu, *et al.* have demonstrated the growth of silica nanoshells around liquid metal droplets using a streamlined sonochemical synthesis approach and their functionality for targeted photonanomedicine.²⁵

We took inspiration from previous work on the colloidal assembly of two-dimensional materials at interfaces of various liquid/liquid systems^{43–48} and sought to expand this capability to liquid metal/water systems. A protective encapsulation can potentially be beneficial for gallium-based liquid metal alloys because gallium is known to aggressively alloy with other metals and create problems for device integration. Graphene has previously been used to inhibit the direct interaction of EGaIn with other metals, but had to be deposited on the surface in a separate step.^{49,50}

In this work, we demonstrate that EGaIn particles can be encapsulated with two dimensional materials such as graphene oxide (GO) using a simple one-pot manufacturing process. We elucidate the mechanisms through which encapsulation occurs by exploring other graphene family materials with different surface chemistries. The utility of this encapsulation is demonstrated through particle integrity in aqueous environments across a wide range of pH and in tunability of mechanical properties of deposited inks. We anticipate this work will broaden the range

of compatible manufacturing processes, materials, and environments for liquid metal particles and to pioneer the exploration of a wide range of new hybrid functional materials composed of 2D materials and liquid metals.

2 Experimental

2.1 Preparation of graphene family materials

To investigate the effect of different chemistries on interactions with liquid metal, several versions of graphene were prepared. Graphene oxide was purchased from the Graphene Supermarket (Ronkonkoma, NY) and used without further modification as the GO material, or was used as the base material for thiolated GO (SHGO) or reduced GO (RGO) preparation. To make the SHGO, the procedure developed by Chua, *et al.* was used.⁵¹ Briefly, 10 mL of HBr was added to 150 mL of a 1 mg/mL GO suspension and stirred for 2 hours at 30°C. Then 10 g of thiourea was added and the solution was warmed to 80°C and stirred for 24 hours under a reflux condenser. The solution was then cooled, and neutralized with sodium hydroxide. The resulting SHGO particles were filtered and washed with ether and an excess of distilled water over a 0.2 μm PTFE membrane. To make the RGO, the acetic/hydroiodic acid reduction method developed by Moon, *et al.* was used.⁵² Briefly, 400 mg of GO was added to 150 mL of glacial acetic acid and sonicated for 30 minutes to ensure dispersion. Then 80 ml of HI acid was added, and the mixture was stirred at 40°C for two days. Once complete, the resulting RGO particles were filtered, neutralized with sodium bicarbonate, and washed with an excess of distilled water and acetone over a 0.2 micron PTFE membrane. The median lateral dimension (d_{50}) for all graphene family materials was determined to be 2 μm , which is congruent with the size distribution of the parent material reported by the vendor. Both the SHGO and RGO were stored as dry powders under vacuum and reconstituted into aqueous solutions as needed for encapsulation experiments.

The atomic percentages of the GO and modified materials were measured using X-ray photoelectron spectroscopy (XPS). However, many carbon-sulfur bonds are similar in energy to carbon-oxygen bonds, which can make determination of the relative atomic percentages difficult. The measured atomic percentages in the SHGO sample by scanning electron microscopy with energy-dispersive X-ray spectroscopy (SEM-EDX) were found to be consistent with those for the literature procedure used,⁵¹ and these numbers are reported in Table 1.

2.2 GaLMA particle synthesis and encapsulation

To make GaLMA particles, approximately 75 wt% of 99.9999% purity Gallium and 25 wt% of 99.9999% purity Indium (Indium Corporation, Clinton, NY) were mixed to form EGaIn. The colloidal suspensions of GaLMA particles were made by sonicating 500 mg of EGaIn (Indium Corporation, Clinton, NY) in 10mL of solvent (water or ethanol). Adjustments to the pH were made using 1M HCl or NaOH solutions as needed. Samples were probe sonicated for 10min with a 1/8 in. microtip at 100 μm amplitude, 20kHz frequency (VCX500 ultrasonicator, 25% amplitude). The vial containing the solvent/EGaIn mixture was immersed in a

chiller bath set to 6° C. The probe tip was located approximately 1.5cm from the bottom of the conical tube. Total energy deposition per sample was 7249 ± 629 J. For the encapsulation experiments, the graphene-based material was added to water to reach a final concentration of 0.5 mg/mL. Adjustments to the pH were made using 1 M HCl or NaOH as needed, and the solutions were bath sonicated for one hour to ensure dispersion of the graphene-based materials. The dispersion of GO or modified version was then used as the solvent for the GaLMA particle synthesis procedure described above. A schematic outlining this process is included in the supplementary information†. The hypoxic experiments were carried out in a nitrogen glovebox and the oxygen concentration maintained was below 10 ppm. Solutions containing GO or the modified versions were degassed by three freeze-pump-thaw cycles in liquid nitrogen under an argon atmosphere.

2.3 Electromechanical investigation

To investigate the electromechanical properties of the GO-coated liquid metal particles, two types of tests were performed: single particle compression and bulk film compression. The single particle compression tests were performed using a custom compression jig inside an SEM (FEI Quanta). Solutions of liquid metal particles were prepared as described above, then diluted prior to spin coating onto a silicon wafer substrate to attain a very sparse distribution of particles. The silicon wafer was affixed to the platen of the compression jig with an epoxy resin. The compression punch was fabricated by ablating a tungsten probe with a focused-ion beam to form a flat compressive counterface with a tip diameter of $\approx 5 \mu\text{m}$. The tip was mounted to a 10 g compressive load cell and was driven by a piezoelectric linear actuator. The particles were compressed at a constant displacement rate of $\approx 0.025 \mu\text{m/s}$ for the GO-coated particles and $\approx 0.049 \mu\text{m/s}$ for the bare particles. SEM images were taken every 5 s during compression.

The bulk film compression tests were performed using a universal testing system (MTS Systems Corp.). Particle solutions were prepared as discussed above then pipetted into custom-made acrylic wells and allowed to dry for at least 24 hours in ambient conditions. Each well was 3 mm deep and 15 mm in diameter and contained two parallel wires embedded in the bottom of the well. The wires were used to measure the resistance of the film during compression, via a voltage divider circuit. The well and a corresponding punch also made of acrylic were secured to the platens using double-sided tape. The film was compressed at a rate of 3 mm/s until a maximum load of 3000 N was reached.

3 Results and Discussion

3.1 Graphene-based material surface interactions with EGaIn particles

The ability of unmodified graphene oxide (GO) to encapsulate the EGaIn surface is shown in Fig. 1. Panel A is an exemplary overview image of liquid metal particles synthesized via sonication in water in the presence of GO. Traditional EGaIn particles stabilized by the native oxide have a very smooth surface morphology; in contrast, the closeup image in panel B shows the

Table 1 Atomic composition (%) of the GO and modified versions

	C	O	S
GO	71.9	23.1	0.4
SHGO	82.6	3.4	14.0
RGO	98.4	1.6	0.0

characteristic wrinkled morphology of multilayer tilings of GO sheets.^{44,53} The larger lateral dimension of the GO means that different regions of the same GO sheet can interact with two separate GaLMA particles. Panels 1C and D are a demonstration of this; a GO sheet has been twisted into a tether between two separate liquid metal particles during the motion induced by sonication.

The presence of GO sheets on the GaLMA particle surface was further confirmed by Raman spectroscopy. Metals cause too much scattering of the incident laser to have a meaningful Raman signal, as can be seen by the data in Fig. 2 (red circles). Carbon materials, in contrast, are marked by two characteristic peaks. The G-band arises from the stretching of the C-C bond in graphitic materials, and is common to all sp^2 carbon systems. The D-band is a vibrational mode associated with edge sites, and indicates disorder in the carbon lattice (e.g. by the inclusion of oxygen-containing functional groups). The GO used in these experiments demonstrates a characteristic spectrum (purple circles in Fig. 2).⁵¹ Liquid metal particles that have been through a light washing step in deionized water after the encapsulation experiment still show the Raman spectrum associated with the GO (black circles in Fig. 2), verifying that the characteristic wrinkled morphology (visible in SEM images) is caused by the association of GO sheets with the GaLMA surface.

To further investigate the interfacial interactions between EGaIn particles and the two dimensional sheets, a panel of graphene-based materials was prepared. Graphene oxide is a particularly complex material that consists of an atomically thin layer of hexagonal lattice of sp^2 bonded carbon, but is functionalized on both faces and around the periphery with oxygen-containing functional groups that impart hydrophilicity.⁵⁴ Carboxyl or vinyl-ogous carboxylic groups are found preferentially on edge and defect sites, and uncharged but polar epoxide and hydroxyl groups are preferentially located on the basal plane.⁵⁵ These functional groups are in spatially fixed domains and form a nanoscale patchwork spanning the particle surface that is typically micrometers in lateral dimension. To investigate the role of GO's functional groups on interactions with liquid metal particles, a reduced graphene oxide (RGO) material was prepared,⁵² with as many of these functional groups as possible removed. A third variation of a graphene-based material containing thiol groups was also prepared, since thiols are known to have a high affinity for interaction with the metal surface.^{17,18,56,57} This was done by converting the native basal alcohol groups on GO to thiols according to the procedure developed by Chua, *et al.*⁵¹ The material produced is hereafter referred to as SHGO, in reference to its sulfur-containing thiol (-SH) moieties. The lateral dimensions of the graphene-based materials have a median (d50) of $2 \mu\text{m}$, and the atomic compositions of the three materials are shown in Ta-

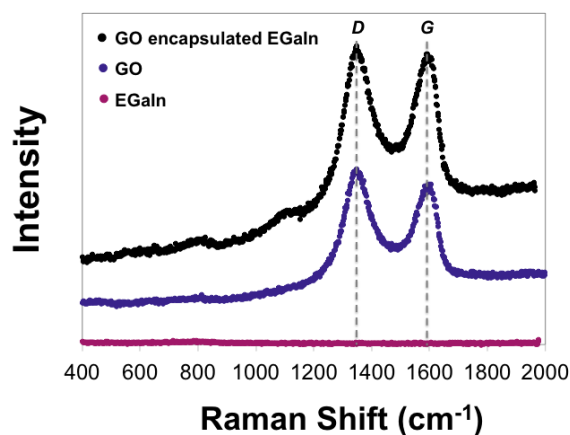


Fig. 2 Raman characterization of GO, EGaIn, and the GO-coated EGaIn particles after the encapsulation experiments. The signature D- and G-bands for carbon materials are marked.

ble 1. Further discussion of the material preparation is detailed in the experimental section, and further characterization of these materials' is available in the supplementary information†.

Fig. 3 provides exemplary images of the interactions between each graphene-based material studied and the EGaIn particles during the ultrasonication fabrication process in water. The GO readily encapsulates the EGaIn particle surface (Fig. 3A), giving the surface a characteristic "rough" appearance that is quite distinct from the native oxide. This roughness is caused by electrostatic repulsions from functional groups on the edges of neighboring GO sheets and basal planes of underlying sheets,⁵⁸ leading them to wrinkle. The morphology is characteristic of both drop-cast multi-layer GO films⁵³ and GO-stabilized Pickering emulsions.⁴⁴ This suggests that the encapsulating film on the LMP surface is composed of multiple GO particles randomly arranged in overlapping layers. In contrast to the GO case, the RGO does not show any evidence of encapsulation (Fig. 3B), multilayer or otherwise. This indicates that the carbon backbone of the materials does not have any affinity to the liquid metal surface, and thus the encapsulation of the EGaIn particles by GO is mediated by the functional groups on the latter.

Despite the well-established affinity between thiols and metal surfaces, the SHGO does not encapsulate the EGaIn surface in the manner of GO under these same experimental conditions. The EGaIn particles in Fig. 3C are smooth and lack the indicative wrinkled morphology of multiple layers of 2D material covering the surface and creating an encapsulation. A small, crumpled SHGO particle can be seen in the top right of the image, separate from the EGaIn surfaces. Some patchy areas on the EGaIn particle surface are visible, which may indicate some interaction of SHGO monolayers, though neither EDX nor Raman spectroscopy could provide persuasive evidence regarding the presence of SHGO on the EGaIn surface (data not shown). The reactivity of EGaIn with dissolved oxygen to produce a passivating surface oxide is well established, and thiols are known to compete with oxygen for metal surface sites.⁵⁶ In this system, the thiols are anchored on

the surface of 2D particles that diffuse extremely slowly in solution (on the order of 10^{-9} cm²/s).⁵⁹ This constraint renders the thiol moieties unable to compete with dissolved molecular oxygen species, which have a diffusion coefficient that is about four orders of magnitude higher than the 2D particles and which are further known for their near-instantaneous reaction with the liquid metal.¹³ Carboxylic acids, which are preferentially found around the edges of GO sheets, are also known to interact with the EGaIn oxide during particle synthesis.⁶⁰ These functional groups survive the modification procedure from GO to SHGO.⁵¹ If the carboxylic acids were predominantly responsible for the interaction with the EGaIn, the same wrinkled morphology of encapsulation would be observed in the SHGO case as it is the GO case, and there would be a clearly measurable Raman signal from the encapsulating shell. This lack suggests that the functional groups on the basal plane of GO (primarily epoxides and hydroxyls) dominate the interaction and allow encapsulation to occur in ambient conditions (Fig. 3A).

To further study how the surface oxide on EGaIn affects the interfacial interactions with the three graphene-based materials, the EGaIn encapsulation experiments were carried out in a nitrogen environmental chamber. Interestingly, it was found that GO also encapsulates the EGaIn in these hypoxic (<10 ppm O₂) conditions (Fig. 3D) as it did in ambient, indicating that the encapsulation behavior of GO is independent of oxygen. We note here that these experiments were conducted in water, which has a significant influence on the surface chemistry of EGaIn.^{40,41} In fact, when a solution of GO in ethanol is prepared and the experiment is repeated in the absence of water, no encapsulation ensues. No encapsulation occurs for any of the graphene-based materials when moved into ethanol (further details shown in Figure S3 of the supplementary information†).

The RGO continues to show no affinity for the EGaIn surface (Fig. 3E) in the hypoxic water as it did in the ambient-atmosphere water, because the RGO does not contain any compatible functional groups to drive the interaction. However, the behavior of SHGO does change between the hypoxic and ambient cases. In the absence of competition from small molecule oxygen species, the SHGO is able to encapsulate the droplets of liquid metal formed during sonication (Fig. 3F). A representative schematic to summarize these different conditions, and when encapsulation does or does not occur, is shown in the center of Figure 3.

In a separate study by our group, GaLMAs have been shown to react with water, leading to the formation and growth of gallium oxide hydroxide (GaOOH) crystallites.⁴⁰ These crystallites form very rapidly in low-oxygen conditions due to a free radical pathway caused by water sonolysis and a lack of competition from dissolved oxygen for metal surface sites. However, no crystallites were observed after the oxygen-free GO encapsulation experiments (Fig. 3D-F). Graphene-family materials are known antioxidants with a particular efficacy towards scavenging and stabilizing the hydroxyl radical.⁶¹ GO and its modified version have sufficient antioxidant activity to inhibit the rapid onset of GaOOH crystallite formation in oxygen-free conditions. The graphene-family materials do not completely quench this reaction, however, as it can still proceed via non-radical pathways. Thus, it is possi-

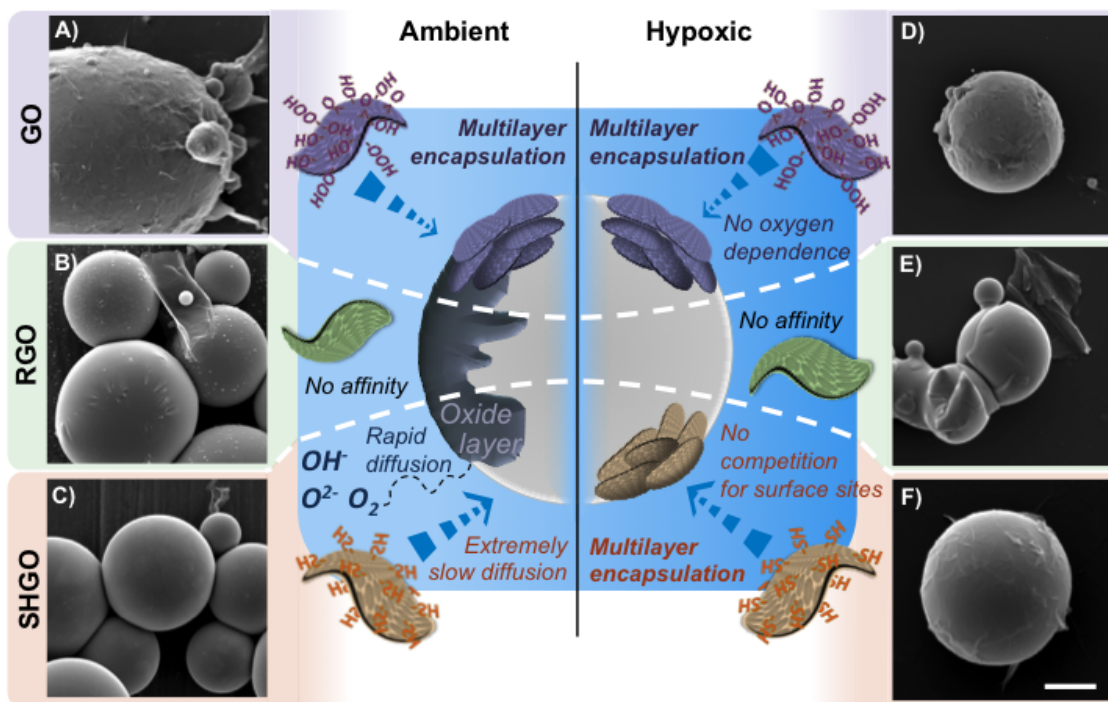


Fig. 3 The morphology of EGaIn particles prepared in the presence of A) GO demonstrate the characteristic wrinkled morphology, but those prepared in the presence of B) RGO or C) SHGO in ambient conditions are smooth, and there is no evidence of interaction between the 2D materials and the liquid metal surface. D) GO can also encapsulate in oxygen-free environments, and so the mechanism must be independent of the presence of oxygen. E) RGO still shows no affinity for the surface in the absence of oxygen. F) The SHGO is able to encapsulate liquid metal droplets in oxygen-free conditions when there is no competition against dissolved oxygen species for surface sites. Scalebar is $2\ \mu\text{m}$ for all micrographs. The schematic in the center summarizes when encapsulation does or does not occur for the graphene-family materials studied.

ble to see crystallites form after the encapsulated LMPs have been left undisturbed in water overnight (see Figure S4 of the supplementary information†). This has significant implications for the stability of the dispersions. In order for the GO encapsulation to ensue, the process must be conducted in an aqueous milieu. However, for practical applications, it will be necessary to subsequently exchange the solvent after processing for ethanol (or another similarly inert solvent) in order to avoid the corrosion of the Ga metal into GaOOH crystallites.

3.2 GO as an environmental barrier

To form EGaIn particles, there must be a physical barrier between adjacent liquid metal droplets in order to inhibit re-coalescence.⁶² This barrier is most commonly in the form of the oxide skin. Strongly acidic and basic environments are known to etch this gallium oxide skin,^{42,63} so colloidal suspensions of EGaIn are not generally stable under these conditions. This is demonstrated in Fig. 4A, which shows a suite of aqueous solutions from pH 0-14 (varied by the addition of HCl or NaOH) with 500 mg of EGaIn that have all been sonicated to induce particle formation of the liquid metal. For pH environments between 3 and 11, the solution turns cloudy from the dispersion of formed liquid metal particles. Within these bounds, the passivating oxide skin is stable, in accordance with the Pourbaix diagram of gallium.⁶⁴ However, as the pH deviates outside this range, the oxide skin providing the stability of the liquid metal particles is etched away resulting in increasingly unstable colloidal suspensions and a greater degree of settling and coalescence. At pH 1 or 13 (0.1M HCl or NaOH, respectively) there is no discrete particle formation and all of the EGaIn is coalesced into a single large bead of bulk liquid metal following sonication (insets in Fig. 4A).

In the absence of the oxide layer, some other barrier must be present to maintain discrete liquid metal particles. Motivated by our earlier success of GO encapsulation in oxygen-free environments, we applied this approach to provide a stable barrier to the EGaIn particles and found that adding GO to the solution prior to sonication yields more stable suspensions across a wider range of pH values, as shown in (Fig. 4B). This includes samples prepared in 0.1M HCl or NaOH, respectively. In these chemically etching environments, any liquid metal particles formed must be due to the stabilizing effects from the GO. It was further found that GO-encapsulated liquid metal particles synthesized at neutral conditions remained stable when strong acid or base was titrated into the vial in order to change the overall pH of the system. This is consistent with the encapsulation experiments conducted in hypoxic conditions, which indicated that the GO encapsulation does not rely on the liquid metal's surface oxide.

In the acidic environment (pH = 1), the GO encapsulating shell shows a notably rougher, more wrinkled surface (Fig. 4C-D) than in a neutral solvent (Fig. 1A, *vide supra*). In the basic environment (pH = 13), the liquid metal initially appears uncoated (Fig. 4E), and evidence of the GO sheets can only be seen at very high magnification (Fig. 4F). These changes in morphology are caused by changes in thickness of the GO film gathering at the LMP surface (verified by XPS measurements; see supplementary informa-

tion†). The behavior of the GO film in acidic conditions is due to a surplus of protons in solution, which complex with the carboxylic acid groups along the periphery of the GO sheets. The loss of charge decreases the electrostatic repulsion between sheets and also renders them more hydrophobic, causing mild aggregation and overlap.⁴³ As the pH increases, the carboxylic groups are deprotonated. The ionized sheets repel each other in solution, and an increasingly sparse coverage is realized on the surface of the EGaIn. At pH 14, the coverage is too sparse to serve as a physical barrier against coalescence, and a single bead of EGaIn can be seen at the bottom of the dark GO dispersion. Due to the significant density differences between the liquid metal, free GO, and the solvent, the dispersions begin to settle immediately after sonication. The samples shown in Fig. 4B were prepared in a random order to avoid bias, but this preparation results in the inhomogeneous appearance of the various solutions as they are each at a different stage of the settling process.

The ability of RGO and SHGO to encapsulate EGaIn in these extreme pH environments was also explored. RGO shows as little affinity for the liquid metal surface in these etching conditions as it does in ambient, rendering it unable to stabilize liquid metal particles throughout the entire range of pH studied. Alternatively, SHGO shows a pH-dependent affinity for the liquid metal surface, and is able to encapsulate in basic but not acidic conditions. Thiols are weak bases and are protonated at low pH, which could inhibit their binding to the EGaIn surface despite the availability of metal surface sites. Instead, SHGO flocculates together, and there is no stable encapsulation of the EGaIn particles. In strongly basic conditions (pH = 13) the oxide is also etched away from the particle surface. However, at the much higher pH, the thiols are predominantly deprotonated and may more readily form thiolate complexes with the exposed EGaIn surface, resulting in stabilized EGaIn particles (Fig. 5). The SHGO still appears flocculated in these basic conditions. This is possibly due to the favorable formation of disulfide bonds in basic conditions which crosslink separate SHGO sheets into stable aggregates, but may also just be an effect of salt-induced aggregation.

3.3 GO as a modifier of electromechanical behavior

Particles of EGaIn and other low melting point alloys have often been used as responsive electrical materials, and are 'activated' (rendered conductive) by applying compression (also referred to as "mechanical sintering"),^{22,65} shear,⁶⁶ or strain²⁰ to rupture the oxide shells and allow the interior molten cores to coalesce. The responsive effect is correlated with particle size^{16,22} and oxide skin thickness.²¹ Here, we evaluate the effect of GO encapsulation on the compression of individual liquid metal particles and on the electromechanical response of deposited films, simulating mechanical sintering. These results can be used to guide processing and handling parameters for future devices fabricated with GO-encapsulated EGaIn particles.

We first evaluated the effect of GO encapsulation on single particle compression mechanics. For these tests, GO-encapsulated particles (prepared in deionized water) and GO-free control particles (prepared in ethanol) of similar size were compressed in

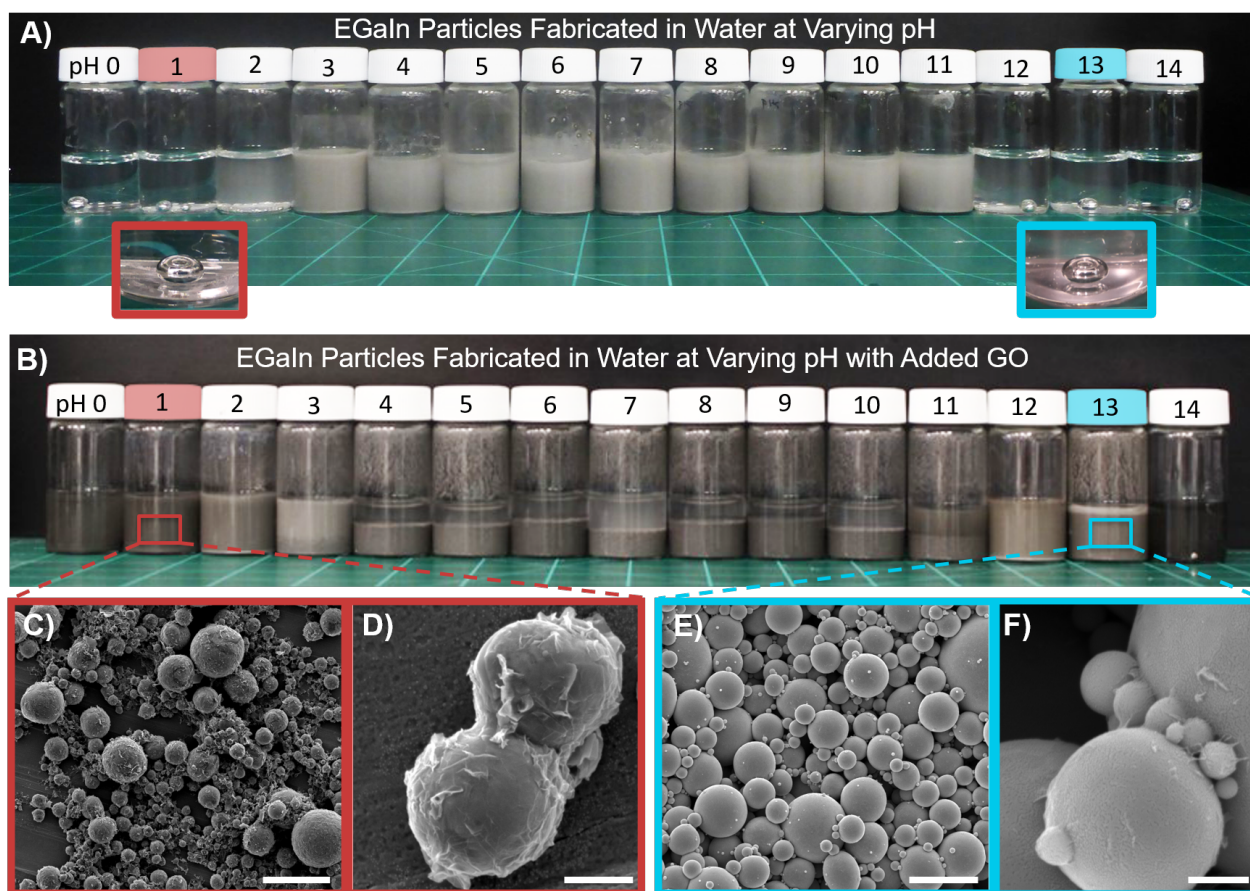


Fig. 4 A) After sonication, solutions of liquid EGaIn in water with pH between 3 and 11 become cloudy as the liquid metal remains discretized into particles. As shown in the insets, in strongly acidic solutions (0.1M HCl), and strongly basic solutions (0.1M NaOH) the liquid metal re-coalesces and doesn't form particles. B) Addition of GO enables formation of particles from pH 0-13. At pH 14, only a single ball of EGaIn can be seen. C-D) SEM images of particles formed in 0.1M HCl solution (scalebar = 20 μm and 0.5 μm, respectively). Wrinkled GO can be seen between the separate liquid metal particles. E-F) SEM images of particles formed in 0.1M NaOH solution (scalebar = 20 μm and 0.5 μm, respectively). The coverage is thinner than in the acidic case, but is still enough to stabilize the individual particle.

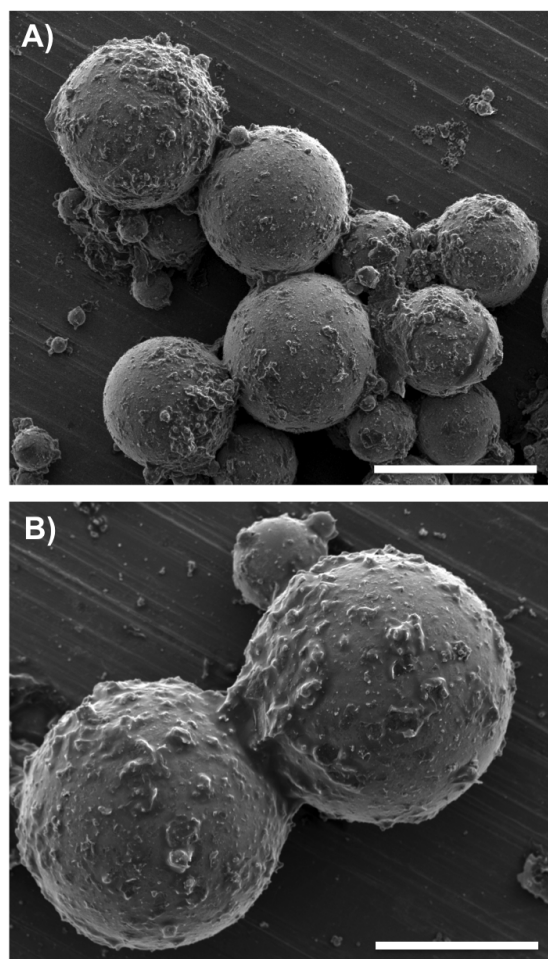


Fig. 5 A) Overview image of the SHGO encapsulation experiment carried out in 0.1M NaOH. Scalebar is 50 μ m. B) Closeup image of an isolated cluster of the encapsulated particles. Scalebar is 20 μ m.

a scanning electron microscope while recording the load and tip displacement (Fig. 6A-C; additional plots and video in supplementary information†). Ethanol was used as the control sample because water has a very high surface tension, and the induced capillary forces on the particles during drying can be quite strong and cause coalescence of neighboring particles.⁶⁷ The sequential SEM images in Fig. 6A and B show the compression of a GO-encapsulated and an unencapsulated particle, respectively. Comparing the particle deformations between these two cases, we can observe slightly more distinct buckling of the exterior shell in the GO-encapsulated particle (most visible in the second images in the sequence), and more prominently, a lack of recovery of the initial particle morphology after releasing the compressive stress (see final images in the sequence). This mechanical behavior is reflected in the load-displacement plot (Fig. 6C). The particle stiffness was calculated using the slope of the load-displacement curve from the point of contact to a displacement equal to 10% of the particle diameter. The GO-encapsulated particle had a stiffness of 59.8 N/m, which was more than 10 \times stiffer than the 4.0 N/m for the unencapsulated particle, which agrees well with previously reported stiffness measurements^{21,22}.

The GO-encapsulated particle data show sequential load-unload peaks that we attribute to multiple buckling events of the GO shell. Near the end of compression, the load-displacement curve of the unencapsulated particle levels off and drops slightly. In contrast, the apparent stiffness for the GO-encapsulated particle increases sharply, due to the compression of mostly GO sheets at the end of the test. Upon unloading, the GO-encapsulated particle recovers to a lesser degree than the control particle (in Fig. 6A and B, the GO-encapsulated particle recovered to 83% original height compared to 95% recovery of the control particle). This behavior is reflected in the load-displacement plots where the control particle exhibits less hysteresis in comparison to the GO-encapsulated particle. Further compression tests on additional particles corroborate the differences in elastic recovery between the GO-encapsulated and unencapsulated particles (see Fig. ?? in the supplementary information).

To complement findings from single-particle compression, a set of EGaIn inks were prepared to gain an understanding of mechanical sintering of macro-scale films. The inks were prepared by sonicating EGaIn in either an aqueous solution of GO or in ethanol (GO-free control). Though all GO-containing samples were prepared in water, a control case of EGaIn particles prepared by sonication in water was not included, because this preparation method resulted in conductive films ($10^{-1} \Omega$) upon drying, without any external compression. As mentioned earlier, water has a very high surface tension, and the induced capillary forces on the particles during drying can be quite strong. This initial conductivity is due to liquid metal particles self-sintering under the high capillary forces induced by water evaporation.⁶⁷ However, when GO is present, it creates a physical barrier at the surface that is more mechanically stable and inhibits coalescence.

The inks were deposited into pre-made acrylic wells with two parallel wires running along the base. The inks were allowed to dry, and the initial resistance across the two wires was measured. The initial resistance of dried GO-encapsulated particle films prior to being subjected to any load was $10^6 \Omega$, while the particles sonicated in ethanol without GO exhibited an initial resistance of $10^9 \Omega$, aligning with previous work.²² The lower initial resistance of the film of GO encapsulated particles could be due to combinations of several possible factors. Some liquid metal particles may have had poor GO coverage and a small degree of water-induced coalescence may have occurred.⁶⁷ GO could also have an effect on the thickness of the gallium oxide, either due to its antioxidant properties⁶¹ or by restricting access of oxygen to the surface.⁴⁵ GO has an intrinsically higher (yet still extremely low) conductivity compared to the native gallium oxide, and could lead to a net decrease in overall interfacial resistances.

The dried films within the acrylic wells were then subjected to a compressive load while recording their electrical resistance via a voltage divider circuit. The results are shown in Fig. 6D. We note here that the variance in measurements is quite large (with coefficient of variations greater than unity for many data points), which is likely due to the large polydispersity of particle size in the inks (see Figure S6 in the supplementary information†). We thus focus primarily on trends, rather than specific resistance values. In the control case, the resistance of ethanol-sonicated particles sharply

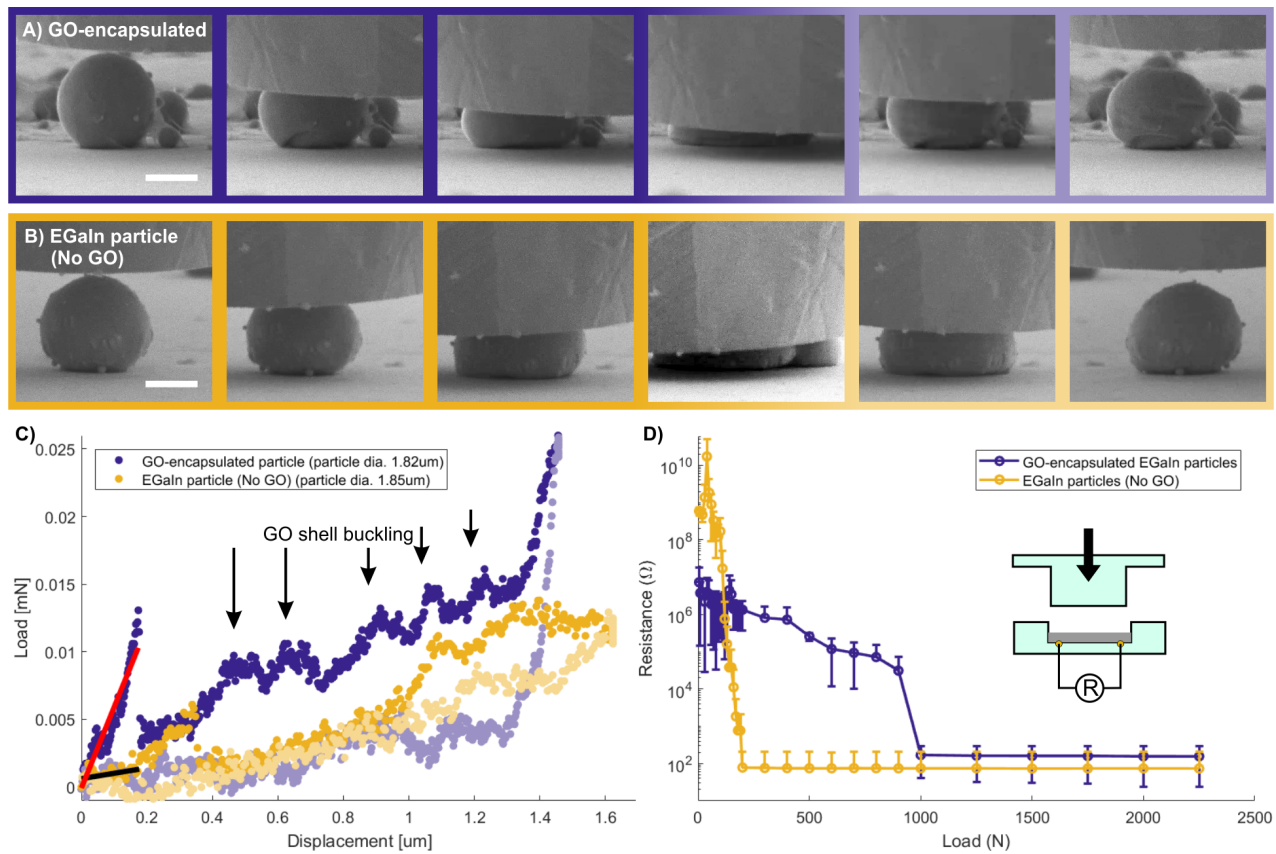


Fig. 6 Electromechanical behavior during compression. A-C) Single particle compression. A) Compression sequence of a GO-encapsulated particle. Note the buckling of the shell visible during compression and even after unloading. Scalebar is $1\mu\text{m}$. B) Compression sequence of an uncoated EGaIn particle sonicated in ethanol. Note the ejection of the liquid metal in the third image and re-uptake of the ejected material after unloading. Scalebar is $1\mu\text{m}$. C) Plot of the force vs. displacement data for two representative tests. The compressive loading is shown in darker colors; the lighter portion of the curve shows the unloading portion of the test. To determine particle stiffness, a linear fit is plotted for the initial compression up to 10% of the particle diameter. D) Electromechanical behavior of bulk films. A schematic of the setup shows a liquid metal film (gray) being compressed by an acrylic punch (light green) inside an acrylic well, through which the resistance is measured. As increasing compressive loads are applied to the deposited films, the particles become mechanically sintered and the electrical resistance decreases. The markers represent mean resistance values measured at specific applied load values, error bars represent 1 standard deviation.

drops 7 orders of magnitude at a compressive load of approximately 50N, indicating coalescence of particles. In contrast, the GO-encapsulated liquid metal particles exhibit a prolonged gradual decrease in resistance as greater loads are applied, followed by a relatively sharp drop in resistance at approximately 900N before stabilizing. Interestingly, the ratio of the load threshold that leads to an onset of conductivity ($900\text{ N} / 50\text{ N} = 18$) is similar to the ratio of individual particle stiffnesses ($60\text{ N/m} / 4\text{ N/m} = 15$) measured above. Initially, the GO shell can deform elastically to withstand this compressive load. However, increased compressive loading leads to buckling of the shell, and cracking and delamination of GO sheets. Failure of both the GO shell and the oxide skin within allows the interior liquid metal to flow out and create a conductive pathway across the bottom of the experimental well.

From the observation that the thickness of the GO shell varies according to pH, two additional solutions were prepared by sonicating EGaIn in GO solutions adjusted to have an acidic or basic pH (1 or 13, respectively), and compared against the results observed here for EGaIn suspensions prepared in neutral conditions. Details can be found in the supplementary information†.

4 Conclusions

In this article, we have demonstrated a robust, scalable, formulation of GO sheets self-assembling into encapsulating films on EGaIn particles. We show that the GO encapsulation process is independent of the presence of oxygen or a native oxide, but is not independent of the presence of water. Water is in fact a primary requirement for this encapsulation, as it influences the EGaIn surface chemistry and creates functional groups to which the hydroxyl and epoxide groups of the GO can attach. These GO encapsulations are especially useful for creating liquid metal colloidal inks in highly acidic and highly basic solvents, which etch away gallium oxides that form on the surface of the EGaIn. The GO forms a physical barrier on the surface of the liquid metal that protects against coalescence. Furthermore, the thickness of the GO encapsulating shell can be tailored by varying the solution pH.

The GO encapsulation also modifies the mechanical behavior of the EGaIn particles. Single particle compression tests reveal that the GO shell increases the overall particle stiffness. These results are paralleled by bulk film compression tests which show that the relationship between particle coalescence, the resistance of the particle film, and compressive load can be tailored with a GO shell. The concept of 2D graphene encapsulation opens up new opportunities for liquid metal systems by broadening the range of functionality, compatible materials, processing environments and methods. Encapsulation by 2D graphene-based materials can potentially unlock opportunities for liquid metal particles by mediating surface interactions, acting as a protective barrier against undesirable environmental factors (e.g. pH, mechanical duress, reactive oxygen species), and providing a platform for further surface functionalization.

Conflicts of interest

There are no conflicts to declare.

Acknowledgements

This research was performed while MAC and MCY held NRC Research Associateship awards at the Air Force Research Lab. The authors would like to thank Daniel Rapping and Robert Wheeler for assistance with mechanical testing.

Notes and references

- 1 Y. J. Tan, J. Wu, H. Li and B. C. K. Tee, *ACS Applied Materials & Interfaces*, 2018, **10**, 15331–15345.
- 2 J. Kang, J. B.-H. Tok and Z. Bao, *Nature Electronics*, 2019, **2**, 144–150.
- 3 E. Palleau, S. Reece, S. C. Desai, M. E. Smith and M. D. Dickey, *Advanced Materials*, 2013, **25**, 1589–1592.
- 4 I. D. Josphipura, H. R. Ayers, G. A. Castillo, C. Ladd, C. E. Tabor, J. J. Adams and M. D. Dickey, *ACS Applied Materials & Interfaces*, 2018, **10**, 44686–44695.
- 5 S. Cheng and Z. Wu, *Lab on a Chip*, 2012, **12**, 2782–2791.
- 6 K. Entesari and A. P. Saghati, *IEEE Microwave Magazine*, 2016, **17**, 50–75.
- 7 S. I. Rich, R. J. Wood and C. Majidi, *Nature Electronics*, 2018, **1**, 102–112.
- 8 N. Lu and D.-H. Kim, *Soft Robotics*, 2013, **1**, 53–62.
- 9 J. Lee, B. L. Zambrano, J. Woo, K. Yoon and T. Lee, *Advanced Materials*, 2020, **32**, 1902532.
- 10 W. Zeng, L. Shu, Q. Li, S. Chen, F. Wang and X.-M. Tao, *Advanced Materials*, 2014, **26**, 5310–5336.
- 11 D.-H. Kim, R. Ghaffari, N. Lu and J. A. Rogers, *Annual Review of Biomedical Engineering*, 2012, **14**, 113–128.
- 12 Y. Liu, M. Pharr and G. A. Salvatore, *ACS Nano*, 2017, **11**, 9614–9635.
- 13 M. D. Dickey, *Advanced Materials*, 2017, **29**, 1606425.
- 14 K. Doudrick, S. Liu, E. M. Mutunga, K. L. Klein, V. Damle, K. K. Varanasi and K. Rykaczewski, *Langmuir*, 2014, **30**, 6867–6877.
- 15 M. H. Malakooti, M. R. Bockstaller, K. Matyjaszewski and C. Majidi, *Nanoscale Advances*, 2020.
- 16 J. W. Boley, E. L. White and R. K. Kramer, *Advanced Materials*, 2015, **27**, 2355–2360.
- 17 L. R. Finkenauer, Q. Lu, I. F. Hakem, C. Majidi and M. R. Bockstaller, *Langmuir*, 2017, **33**, 9703–9710.
- 18 J. N. Hohman, M. Kim, G. A. Wadsworth, H. R. Bednar, J. Jiang, M. A. LeThai and P. S. Weiss, *Nano letters*, 2011, **11**, 5104–5110.
- 19 J. Yan, M. H. Malakooti, Z. Lu, Z. Wang, N. Kazem, C. Pan, M. R. Bockstaller, C. Majidi and K. Matyjaszewski, *Nature nanotechnology*, 2019, **14**, 684–690.
- 20 C. J. Thrasher, Z. J. Farrell, N. J. Morris, C. L. Willey and C. E. Tabor, *Advanced Materials*, 2019, **31**, 1903864.
- 21 N. J. Morris, Z. J. Farrell and C. E. Tabor, *Nanoscale*, 2019, **11**, 17308–17318.
- 22 T. R. Lear, S.-H. Hyun, J. W. Boley, E. L. White, D. H. Thompson and R. K. Kramer, *Extreme Mechanics Letters*, 2017, **13**, 126–134.
- 23 J. Zhang, R. Guo and J. Liu, *Journal of Materials Chemistry B*, 2016, **4**, 5349–5357.
- 24 Y. Lu, Y. Lin, Z. Chen, Q. Hu, Y. Liu, S. Yu, W. Gao, M. D. Dickey and Z. Gu, *Nano Letters*, 2017, **17**, 2138–2145.
- 25 P. Zhu, S. Gao, H. Lin, X. Lu, B. Yang, L. Zhang, Y. Chen and J. Shi, *Nano letters*, 2019, **19**, 2128–2137.
- 26 A. Elbourne, S. Cheeseman, P. Atkin, N. P. Truong, N. Syed, A. Zavabeti, M. Mohiuddin, D. Esrafilzadeh, D. Cozzolino, C. F. McConville, M. D. Dickey, R. J. Crawford, K. Kalantar-Zadeh, J. Chapman, T. Daeneke and V. K. Truong, *ACS Nano*, 2020, **14**, 802–817.
- 27 S. A. Chechetka, Y. Yu, X. Zhen, M. Pramanik, K. Pu and E. Miyako, *Nature Communications*, 2017, **8**, 15432.
- 28 R. Zheng, Z. Peng, Y. Fu, Z. Deng, S. Liu, S. Xing, Y. Wu, J. Li and L. Liu, *Advanced Functional Materials*, 2020, **30**, 1910524.
- 29 M. Mayyas, H. Li, P. Kumar, M. B. Ghasemian, J. Yang, Y. Wang, D. J. Lawes, J. Han, M. G. Saborio, J. Tang, R. Jalili, S. H. Lee, W. K. Seong, S. P. Russo, D. Esrafilzadeh, T. Daeneke, R. B. Kaner, R. S. Ruoff and K. Kalantar-Zadeh, *Advanced Materials*, n/a, 2001997.
- 30 W. Zhang, J. Z. Ou, S.-Y. Tang, V. Sivan, D. D. Yao, K. Latham, K. Khoshmanesh, A. Mitchell, A. P. O'Mullane and K. Kalantar-zadeh, *Advanced Functional Materials*, 2014, **24**, 3799–3807.
- 31 W. Zhang, B. S. Naidu, J. Z. Ou, A. P. O'Mullane, A. F. Chrimes, B. J. Carey, Y. Wang, S.-Y. Tang, V. Sivan, A. Mitchell, S. K. Bhargava and K. Kalantar-zadeh, *ACS Applied Materials & Interfaces*, 2015, **7**, 1943–1948.
- 32 L. Ren, X. Xu, Y. Du, K. Kalantar-Zadeh and S. X. Dou, *Materials Today*, 2019.
- 33 G. McHale and M. I. Newton, *Soft Matter*, 2015, **11**, 2530–2546.
- 34 Y. Chen, T. Zhou, Y. Li, L. Zhu, S. Handschuh-Wang, D. Zhu, X. Zhou, Z. Liu, T. Gan and X. Zhou, *Advanced Functional Materials*, 2018, **28**, 1706277.
- 35 V. Sivan, S.-Y. Tang, A. P. O'Mullane, P. Petersen, N. Eshtiaghi, K. Kalantar-zadeh and A. Mitchell, *Advanced Functional Materials*, 2013, **23**, 144–152.
- 36 M. D. Dickey, *ACS Applied Materials & Interfaces*, 2014, **6**, 18369–18379.
- 37 K. Kalantar-Zadeh, J. Tang, T. Daeneke, A. P. O'Mullane, L. A. Stewart, J. Liu, C. Majidi, R. S. Ruoff, P. S. Weiss and M. D. Dickey, *ACS Nano*, 2019, **13**, 7388–7395.
- 38 T. Daeneke, K. Khoshmanesh, N. Mahmood, I. A. d. Castro, D. Esrafilzadeh, S. J. Barrow, M. D. Dickey and K. Kalantar-zadeh, *Chemical Society Reviews*, 2018, **47**, 4073–4111.
- 39 S. Chen, H.-Z. Wang, R.-Q. Zhao, W. Rao and J. Liu, *Matter*, 2020, **2**, 1446–1480.
- 40 M. Creighton, M. Yuen, M. Susner, B. Maruyama and C. Tabor, 2020.
- 41 M. R. Khan, C. Trlica, J.-H. So, M. Valeri and M. D. Dickey, *ACS applied materials & interfaces*, 2014, **6**, 22467–22473.
- 42 R. A. Bilodeau, D. Y. Zemlyanov and R. K. Kramer, *Advanced Materials Interfaces*, 2017, **4**, 1600913.

- 43 L. J. Cote, J. Kim, Z. Zhang, C. Sun and J. Huang, *Soft Matter*, 2010, **6**, 6096–6101.
- 44 M. A. Creighton, Y. Ohata, J. Miyawaki, A. Bose and R. H. Hurt, *Langmuir*, 2014, **30**, 3687–3696.
- 45 M. A. Creighton, W. Zhu, F. van Krieken, R. A. Petteruti, H. Gao and R. H. Hurt, *ACS nano*, 2016, **10**, 2268–2276.
- 46 Q. Luo, Y. Wang, E. Yoo, P. Wei and E. Pentzer, *Langmuir*, 2018, **34**, 10114–10122.
- 47 Q. Luo, P. Wei, Q. Huang, B. Gurkan and E. B. Pentzer, *ACS applied materials & interfaces*, 2018, **10**, 16707–16714.
- 48 B. J. Rodier, C. Hemmingsen, E. Pentzer *et al.*, *Polymer Chemistry*, 2018, **9**, 1547–1550.
- 49 E. B. Secor, A. B. Cook, C. E. Tabor and M. C. Hersam, *Advanced Electronic Materials*, 2018, **4**, 1700483.
- 50 P. Ahlberg, S. H. Jeong, M. Jiao, Z. Wu, U. Jansson, S.-L. Zhang and Z.-B. Zhang, *IEEE Transactions on Electron Devices*, 2014, **61**, 2996–3000.
- 51 C. K. Chua and M. Pumera, *ACS nano*, 2015, **9**, 4193–4199.
- 52 I. K. Moon, J. Lee, R. S. Ruoff and H. Lee, *Nature communications*, 2010, **1**, 1–6.
- 53 F. Guo, G. Silverberg, S. Bowers, S.-P. Kim, D. Datta, V. Shenoy and R. H. Hurt, *Environmental science & technology*, 2012, **46**, 7717–7724.
- 54 D. R. Dreyer, S. Park, C. W. Bielawski and R. S. Ruoff, *Chemical society reviews*, 2010, **39**, 228–240.
- 55 D. C. Marcano, D. V. Kosynkin, J. M. Berlin, A. Sinitskii, Z. Sun, A. Slesarev, L. B. Alemany, W. Lu and J. M. Tour, *ACS nano*, 2010, **4**, 4806–4814.
- 56 Z. J. Farrell and C. Tabor, *Langmuir*, 2018, **34**, 234–240.
- 57 A. Yamaguchi, Y. Mashima and T. Iyoda, *Angewandte Chemie International Edition*, 2015, **54**, 12809–12813.
- 58 L. J. Cote, F. Kim and J. Huang, *Journal of the American Chemical Society*, 2009, **131**, 1043–1049.
- 59 Y. T. Chen, F. Guo, A. Jachak, S. P. Kim, D. Datta, J. Y. Liu, I. Kulaots, C. Vaslet, H. D. Jang, J. X. Huang, A. Kane, V. B. Shenoy and R. H. Hurt, *Nano Lett*, 2012, **12**, 1996–2002.
- 60 I. D. Tevis, L. B. Newcomb and M. Thuo, *Langmuir*, 2014, **30**, 14308–14313.
- 61 Y. Qiu, Z. Wang, A. C. Owens, I. Kulaots, Y. Chen, A. B. Kane and R. H. Hurt, *Nanoscale*, 2014, **6**, 11744–11755.
- 62 T. Daeneke, K. Khoshmanesh, N. Mahmood, I. De Castro, D. Esrafilzadeh, S. Barrow, M. Dickey and K. Kalantar-Zadeh, *Chemical Society Reviews*, 2018, **47**, 4073–4111.
- 63 S.-Y. Tang, V. Sivan, K. Khoshmanesh, A. P. O'Mullane, X. Tang, B. Gol, N. Eshtiaghi, F. Lieder, P. Petersen, A. Mitchell *et al.*, *Nanoscale*, 2013, **5**, 5949–5957.
- 64 Y. Chung and C.-W. Lee, *J. Electrochem. Sci. Technol*, 2013, **4**, 1–18.
- 65 B. J. Blaiszik, S. L. Kramer, M. E. Grady, D. A. McIlroy, J. S. Moore, N. R. Sottos and S. R. White, *Advanced Materials*, 2012, **24**, 398–401.
- 66 M. D. Bartlett, N. Kazem, M. J. Powell-Palm, X. Huang, W. Sun, J. A. Malen and C. Majidi, *Proceedings of the National Academy of Sciences*, 2017, **114**, 2143–2148.
- 67 M. C. Yuen, M. A. Creighton and C. E. Tabor, 2020 IEEE International Conference on Soft Robotics (RoboSoft), 2020, pp. 000–000.